High precision Sr, Nd, and Pb isotopic analyses using the new generation Thermal Ionisation Mass Spectrometer ThermoFinnigan Triton-Ti®

Riccardo Avanzinelli[1*], Elena Boari[1], Sandro Conticelli[1,2], Lorella Francalanci[1,2], Luisa Guarnieri[1], Giulia Perini[1], Chiara M. Petrone[1], Simone Tommasini[1,2] and Maurizio Ulivi[1]

[1] Dipartimento di Scienze della Terra, Università degli Studi di Firenze, Via Giorgio La Pira, 4, I-50121, Firenze, Italy
[2] Istituto di Geoscienze e Georisorse, Sezione di Firenze, Consiglio Nazionale delle Ricerche,
Via Giorgio La Pira, 4, I-50121, Firenze, Italy

Abstract. — The new generation Thermal Ionisation Mass Spectrometer (ThermoFinnigan Triton-Ti®) and a clean lab for sample preparation have been established in Firenze in the last few years. Our research group has carried out the calibration of the analytical methods and the technical procedures to be applied in a number of geological research fields. In this contribution, we present the analytical procedures set up in the Radiogenic Isotope Geology Laboratory of Firenze with particular attention to the instrumental methodologies utilised in order to obtain high performances in terms of precision and accuracy on the measurement of Sr, Nd, and Pb reference samples.

Riassunto. — A Firenze sono stati recentemente installati uno spettrometro di massa di nuova generazione (ThermoFinnigan Triton-Ti®) ed un laboratorio di chimica fine per la purificazione dei campioni. Il nostro gruppo di ricerca ha sviluppato e messo a punto procedure analitiche applicabili nei diversi campi delle scienze della terra. In questo contributo sono presentate le procedure analitiche messe a punto nel Laboratorio di Geochimica degli Isotopi Radiogenici di Firenze, con particolare attenzione alle metodologie strumentali utilizzate allo scopo di ottenere la produzione di misure isotopiche di alto livello, in termini di precisione ed accuratezza, su standard internazionali di Sr, Nd e Pb.

* Corresponding author, E-mail: riccardo.avanzinelli@geo.unifi.it

Introduction

Isotope Geology had a great development in the last fifty years thanks to the technologic development of mass spectrometer equipments. Last generation mass spectrometers gave a new impulse to the isotopic research in the Earth Sciences, providing the possibility to strongly reduce the analytical time and concomitantly increasing accuracy and precision. In the present paper we report data on a set of international certified standard materials and intra-lab reference samples, used as secondary standards, to evaluate the quality of the data produced in our laboratory, namely: the NIST SRM 987 for Sr isotopes, the La Jolla and NdFi for Nd isotopes, and the NIST SRM 981 for Pb isotopes. Particular attention has been dedicated to dynamic versus static measurement strategies and to the proper selection of the model used for the correction of mass fractionation effects. On the basis of the obtained data, the analytical philosophy and the selection of measurement type and fractionation law corrections have been discussed in the light of achieving the smallest standard error of the measurements. In particular the analytical methods have been calibrated to

assess small isotopic variations in ongoing lava flows and eruptions in active volcanoes in order to accurately monitor changes in the feeding system during eruptions. The possibility of performing high precision analyses on extremely small-size samples will also enable in-situ isotopic determinations on mineral phases (microdrilling technique) to study intra-grain variations and investigate pre-eruptive mechanisms in quiescent volcanoes.

The Mass Spectrometer

The ThermoFinnigan Triton-Ti® (Fig. 1) magnetic sector field thermal ionisation mass spectrometer (TIMS) separates charged atoms or molecules on the basis of their momentum along their way through the magnetic sector field. The ion optics of the Finnigan TRITON is based on a magnetic sector field, which deflects the ion beam by 90 degrees. This geometry ensures a compact setup of the system and a small footprint. In its principles it is still very similar to the very first designs of Alfred Nier. A "Nier-type" mass spectrometer (Nier, 1940; 1947) consists of three parts, which are evacuated to 10^{-7} - 10^{-9} mbar: (i) an ion source to produce positively or negatively charged ions with a very narrow energy spread (ii) a magnetic sector analyser (of 60° ion deflection; Nier, 1940), and (iii) a detector to collect the mass separated ions. The solid samples, usually in the form of a salt of the element, are deposited onto a filament (composed of Re, W, or Ta) and then mounted into the evacuated ion source housing of the mass spectrometer. The filament is heated by an electrical current of several Ampere flowing through the filament to a temperature sufficient to evaporate the element to be analysed. In case of a double filament sample, there is a second filament, adjacent to the sample filament, which is called the ionization filament. The ionization filament usually is heated to very high temperatures up to 2000 °C. The atoms evaporating from the sample filament and hitting directly onto the hot surface of the ionization filament are ionised by a charge transfer to the surface of the ionization filament. The resulting ions are then accelerated by a high electric extraction field strength and subsequently focused by an ion source lens stack, consisting of
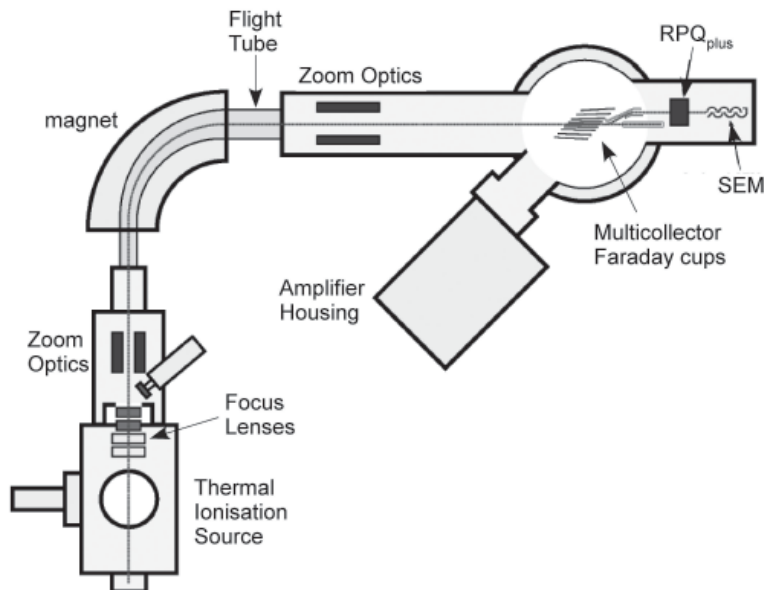

Fig. 1 – Schematic outline of the state-of-the-art Thermal Ionisation Mass Spectrometer (TIMS), ThermoFinnigan Triton-Ti® (used with permission of ThermoFinnigan).

a set of suitably spaced slit plates, to a rectangular shaped ion beam onto the entrance slit of the mass spectrometer. Finally, the ion beam enters a magnetic field which is oriented perpendicular to the travel direction of the ion beam. The magnetic field is generated by an electromagnet whose pole pieces are specially shaped to minimise ion optical aberrations and to produce a sharp image in the focal plane of the mass spectrometer. The magnetic field deflects the ions into circular paths whose radii are proportional to the square root of the masses of the different isotopes. Thus different isotopes of one element travel along different radii and appear at different positions along the focal plane of the mass spectrometer. The separated ion beams travel in a so-called flight tube, which is evacuated to high vacuum (ca. $3\text{-}4\cdot10^{-9}$ mbar) to reduce collisions of the ions with residual gas, and eventually arrive to the collector (Faraday cup). The Faraday cups of Triton-Ti® consist of a graphite cup positioned behind a slit plate. The ThermoFinnigan Triton-Ti® uses a variable multicollector, which supports 8 motorised and moveable Faraday cups plus one fixed Faraday cup, which can be positioned to catch all isotopes of one element simultaneously. The beam that enters the collector cup is neutralised by electrons that flow from ground to the collector through a feedback resistor (usually $10^{11}\Omega$) of the current amplifier. The output voltage of this current amplifier is measured with a digital voltmeter. For example, with a $10^{11}\Omega$ feedback resistor, an ion beam current of $5\cdot10^{-11}$ A generates a signal of 5 V.

The ThermoFinnigan Triton-Ti® (e.g., Wieser and Schwieters, 2005) (Fig. 1) in use in Firenze is the latest generation solid-source thermal ionisation mass spectrometer designed to work in complete remote control and suited to produce positive or negative ions. The instrument is equipped with an ultra-high abundance sensitivity Retarding Potential Quadrupole (RPQ$_{plus}$®) filter installed on the central ion counting channel. The sample wheel has 21 positions, the linearity of the collectors range from 0 to 50 V, and the connection system of amplifiers and Faraday cups is not fixed (*Virtual Amplifier*).

One of the most peculiar features of this instrument is the high analytical sensitivity of the ion source. The shape of the electrical lenses has been optimised in order to minimise contamination of the ion source due to beam exposure. The magnet has an effective dispersion of 810 mm and provides up to 16% mass dispersion. The laminated magnet allows fast peak jumping and the magnetic field can be adjusted in such a way to give a mass range from 1 to 280 a.m.u. when the high voltage is 10 kV. An extended mass range up to 350 a.m.u. can be obtained with a high voltage at 8 kV. A new feature, the dynamic Zoom Optics placed after the magnet, enables the user to slightly change the dispersion of the mass analyser, thus ensuring maximum peak overlap and enhancing the precision attainable with multi-dynamic measurements.

The multi-collector system hosts 9 Faraday cups, of which 8 can be freely positioned with high precision. The Faraday cups have a dynamic range of 50 V ($10^{11}\Omega$). This multi-collector set allows for simultaneous measurement up to 9 separate isotopes. The centre channel slit is fixed, and the ion beam can be deflected either into a Faraday cup or a dynode of a Secondary Electron Multiplier (SEM). An ultra-high abundance sensitivity Retarding Potential Quadruple filter (RPQ$_{plus}$®) is present prior to the axial ion counter (SEM) (Fig. 1). Collectors may be positioned to measure isotopes at unit mass intervals for elements ranging from Lithium to Uranium and Plutonium. A maximum mass difference of 16 % can be accommodated across the collector array. The focal plane is oriented at 45° to the axial beam.

The Faraday cups have narrow entrance slits. The inclined inner walls of the cups are specially coated and shielded to prevent re-emitting ions from the cups. The depth of the Faraday has been increased to increase reliability and consist out of a new material, which is specially conditioned for uniform performance. Each ion current measuring channel (Faraday cup) is provided with an amplifier and voltage to frequency converter package (V/F). The amplifier housing is temperature controlled at ± 0.01°C (ca. 36°C in our mass spectrometer) and under vacuum (~10^{-3} mbar) to ensure a maximum stability and low drift of the electronics (<5 µV per hour). Using an integration period of 64 second with a 10^{11} Ω resistor, the amplifiers have a noise level equivalent to $5\cdot10^{-17}$ A. Linearity of each ion current amplifier is determined mainly by the feedback resistor. The feedback resistors have very low temperature coefficients, <300 ppm/°C, and negligible voltage coefficients. A special constant

current device assures an inter-channel calibration accuracy <10 ppm. A new feature in the design of the Triton-Ti®, is the elimination of the fixed connection of amplifier and Faradays cups. The connection of cups and amplifiers can be switched alternately in a predefined order at the end of a block measurement (*Virtual Amplifier*). This ensures that all cups are using all amplifiers and allows the variable errors in gain calibration factors and the error propagation into the calculated ratios to be cancelled out.

The measurement of the ion beam in analog mode with a Faraday cup is limited by the signal to noise ratio. For signals with intensities ≤ 100 μV (10^{-15} A with a 10^{11} Ω resistor) it is preferred to use a Secondary Electron Multiplier (SEM) for ion counting instead of a Faraday Cup. Due to the superior signal to noise ratio for small signals the SEM detector provides a higher accuracy and precision compared to Faraday Cups. The limitation of the ion counter is given by the detection of a single ion, i.e. the charge of $1.6 \cdot 10^{-19}$ C. The impact of an ion on the first dynode of the multiplier structure generates about 4-5 secondary electrons. These electrons are attracted and acellerated onto the following dynodes of the dynode structure and are further multiplied by a factor of 2-3 with each dynode. The SEM itself has 19 dynodes. The dynodes are arranged in a cascade, which leads to a multiplication of every incoming electron in each stage. The typical overall gain is in the range of 10^6,-10^7 meaning that every incoming electron is multiplied by one to 10 million.

Extreme isotope ratios ($>10^5$) can only be determined if the mass spectrometer is able to suppress peak tail contribution of the major isotope to the reading of the minor isotope. The peak tail typically is generated by scattering events of the ion beam along its way from the source slit to the detector slit. The scattering events are generated by scattering on aperture edges and residual gas particles in the evacuated mass analyzer housing. The latter results into the requirement of ultra high vacuum in the mass analyzer. The peak tail contribution of an adjacent mass in the mass spectrum known as *abundance sensitivity*. The Retarding Potential Quadrupole (RPQ$_{plus}$®) is an electrostatic filter lens, which is installed right before the axial detector and it boosts the abundance sensitivity of the Triton-Ti® from ca. 2

ppm to <10 ppb at mass 237 (^{238}U tail) and <5 ppb at mass 230 (^{232}Th tail)(ThermoFinnigan, personal commucation). The abundance sensitivity, apparent in the so-called peak tails, is affected mainly by the interaction of ion with residual gas in the analyser or by scattering of ions at slits, apertures or other beam limiting items. As a consequence of these scattering processes, the ions suffer some kinetic energy loss and/or are scattered into incorrect flight angles. These ions do not arrive at their correct mass position on the analyser focal plane. They are collected at adjacent masses and contribute to the background. The RPQ$_{plus}$® filter is specifically designed to suppress the contribution of the major isotope to the reading of the minor isotope (e.g., tail of ^{232}Th on ^{230}Th peak), because it rejects scattered ions by both their lower kinetic energy and their irregular flight paths.

Although the SEM and RPQ$_{plus}$® are not necessary for the procedures described in this contribution, their presence is fundamental for the future development of our laboratory, in particular for enabling the measurements of U and Th isotopes, which will be set up and established in the next future.

SAMPLE PREPARATION

Geologic samples for mass spectrometer analyses are prepared in a clean chemistry laboratory equipped with conditioned (ca. 20°C) and over-pressured air ("Class 1000" environment). Sample digestion is performed using a horizontal HEPA-filtered laminar flow work-station sited inside a fume cupboard, which ensures a low-blank working area. Subsequent sample chromatography is performed within a vertical HEPA-filtered laminar flow hood ("Class 100" environment).

High purity chemical reagents and water are used during sample treatment. Concentrated HNO_3 (65-69 wt. %) and HF (40-49 wt. %) are of supra- (Sr and Nd) and ultra-pure (Pb) quality. Concentrated HCl (37 wt. %) of Pro-Analysis quality is distilled using a Quartz sub-boiling distillation device. Water is treated with two steps of purification to obtain high resistivity Milli-Q® water (18.2 MΩ per cm).

PFA beakers are carefully cleaned. They are sub-boiled in a 1:1 solution of HNO_3 and deionised water, rinsed with deionised water, sub-boiled again in a 1:1 solution of HCl and deionised

water, and then rinsed with with Milli-Q® water. Eventually each PFA beaker is filled up with 6N HCl and heated at 140°C on a hot-plate within a fume hood for 1-2 days.

Finely powdered rocks and minerals (<50 mg) are digested in cleaned PFA beakers using a 1:4 mixture of concentrated HNO_3 and HF (e.g., Croudace, 1980). After 1-2 days on the hotplate (140°C), solutions are evaporated to dryness, nitrated twice, dissolved again in 6N HCl on hotplate (120°C), and eventually evaporated to dryness.

Rb, Sr, Sm, and Nd fractions are purified using conventional cation exchange chromatography (e.g. Crock et al., 1984). A previously centrifuged, 0.5 ml of 2.5N HCl sample solution is loaded onto 3.7 ml pure quartz column of AG50Wx8 cation exchange resin (200-400 mesh, Bio-Rad®). Rb, Sr, and Rare Earth Elements (REE) are sequentially eluted with 2.5N HCl (Rb and Sr) and 6N HCl (REE). Columns and resins are cleaned with 6N HCl and Milli-Q® water and then conditioned with 2.5N HCl.

Sr purification of samples, for which REE fraction is not requested, can be also achieved by Extraction Chromatography using 140 µl pure quartz micro-column of pre-cleaned Sr-Resin (100-150 µm, Eichrom®). A new Sr-Resin aliquot is used for each sample. Matrix elements are eluted with 30 CV (Column Volumes) of 3N HNO_3 and Sr is then extracted with 10 CV of Milli-Q water.

Total procedure Sr blank is tested using an [84]Sr (>80%) spike at a concentration of 0.92 ppb and its value is between 120 and 300 pg.

REE fraction is then loaded onto 1 ml pure quartz column packed with Ln-Resin (100-150 µm, Eichrom®) made by teflon coated with di-(2-ethylhexyl) ortho-phosphoric acid (HDEHP resin) (e.g. Richard et al., 1976). Nd and Sm are sequentially eluted with 0.18N and 0.3N HCl (Nd), and 0.5N HCl (Sm). Columns and resin cleaning is obtained by alternating Milli-Q water and 7N HNO_3, rinsing with 6N HCl and then conditioning with 0.18N HCl.

Pb purification is also achieved by Extraction Chromatography using ultra-pure quality acids, and the same micro-columns of Sr-Resin such as for Sr (e.g., Deniel & Pin, 2001). The Sr-Resin is thoroughly pre-cleaned using alternating 6N HCl, 2N HNO_3, and Milli-Q water, and then conditioned with 5 CV of 2N HNO_3. The sample is loaded and washed with 7 CV of 2N HNO_3. Ba and Sr are then eluted with 10 CV of 7N HNO_3 and 2 CV of 2N HNO_3 (Ba), and 10 CV of Milli-Q water (Sr). Pb is eventually extracted with 15 CV of 6N HCl. The column yield for Pb is ca. 90%.

<center>INSTRUMENTAL PROCEDURES</center>

Isotopic fractionation during measurement

Thermal ionisation relies on the production of atomic ions at the hot surface of a metal filament. An ion source with single, double or triple filament arrangement is used for the evaporation and ionisation processes. Using a single filament ion source, the evaporation and ionisation processes of the sample to be analysed takes place on the same filament surface. In the case of a double or triple filament ion source, one or two filaments are used for the evaporation of the sample and the cloud of atoms formed hits onto the surface of the other filament (ionisation). Then, after an electron transfer from the atoms to the filament, the positive ions produced desorb from the filament surface and enter the ion optics system where the ions are accelerated and focused. A double, or triple, filament is advantageous for some elements since it separates the evaporation process from the ionisation process. In particular this is true for the analysis of elements that can be evaporated at low temperature, but which have a rather high first ionisation potential and thus requires a high filament temperature to reach sufficient ion yields (i.e., Nd, Th). The quantitative correlation between the ion production and the physical parameters responsible for this ionisation process (e.g., Denbigh, 1971) demonstrated that the fraction evaporated and ionised is a complex function of the first ionisation potential of the analyte, temperature, and work-function of electrons for the filament material. High yields of ions can be obtained for atoms with low ionisation potential and a high electron work-function of the filament material. The process of evaporation and ionisation is driven by kinetics and requires the breaking of chemical bonds, whose strength is mass dependent. The difference in bond energy between two isotopes of the same element implies that the chemical bond of the lighter isotope is more readily broken than that of the heavier isotope, hence the lighter isotope is

preferentially released from the filament, causing isotopic fractionation. Since the sample loaded on the filament is a finite reservoir, the process of evaporation starts to use up preferentially the lighter isotope so that the isotopic composition of the sample gets progressively heavier with time.

This effect has been widely investigated and several theories have been considered to account for isotopic fractionation during mass spectrometry analysis (e.g., Eberhart et al., 1964; Russel et al., 1978). Eberhart et al. (1964) showed that the evaporation process follows a Rayleigh distillation law, whilst Russel et al. (1978) proposed a slight different model, which takes into account the actual weight of the masses of the different isotopes (i.e. *exponential law*). A number of empirical fractionation laws (i.e., linear law, power law, and exponential law) have been suggested, and are commonly used to correct for this undesirable mass-dependent fractionation effect, which may lead to an error of up to 1% in measured isotope ratios. *Linear* and *power* law are based on the theoretical Rayleigh distillation law, whilst exponential law derives from the study of Russel et al. (1978). These different laws are outlined in Appendix 1 and they can be applied successfully to elements with two or more non-radiogenic isotopes, such as Sr and Nd.

Thirlwall (1991) demonstrated that Sr evaporation from a Ta filament occurs as the metal species Sr and the exponential law correction can account adequately for it. Habfast (1983) suggested, however, that a Sr sample on a Re filament might evaporate as a species such as $SrReO_4$ rather than atomic Sr. The apparent mass of ^{88}Sr, which should be used in the exponential correction, would be *ca.* 330 rather than 88. Under such conditions the exponential law correction might actually produce a worse fit to the true fractionation behaviour of the sample than the linear law. To test this hypothesis, we have carried out a number of measurements to assess the best fractionation law correction for Sr samples that are loaded with a Ta activator and H_3PO_4 on a single Re filament.

Each sample of NIST SRM987 standard, representing a Sr aliquot of either 100 ng or 300 ng, has been measured several times to check the variation, if any, of $^{87}Sr/^{86}Sr$ at different $^{88}Sr/^{86}Sr$ values, i.e. the degree of fractionation. The average $^{88}Sr/^{86}Sr$ of each run ranges from 8.31

to 8.45 (Table 1) and cover most of the values commonly observed in measurement of unknown samples. The two different $^{87}Sr/^{86}Sr$ values reported in table 1 represent the ratios corrected using a linear fractionation law (*lfl*), and an exponential fractionation law (*efl*), respectively. The two average values are virtually identical, although the external reproducibility is considerably better for $^{87}Sr/^{86}Sr_{efl}$ (0.710251 ± 11, 2σ, n = 22) than for $^{87}Sr/^{86}Sr_{lfl}$ (0.710253 ± 28, 2σ, n = 22). This can be better appreciated in figure 2a, where the two sets of $^{87}Sr/^{86}Sr$ are compared *vs.* the average $^{88}Sr/^{86}Sr$ of individual runs. The $^{87}Sr/^{86}Sr_{efl}$ remains constant, within run precision, whereas $^{87}Sr/^{86}Sr_{lfl}$ tends to increase slightly with increasing the degree of fractionation (i.e., $^{88}Sr/^{86}Sr$). The linear fractionation correction does not produce a stable isotope ratio over time, which means it does not fully correct for the time dependent variation of the raw isotope ratio. Whereas the exponential correction produces a stable isotope ratio over time and thus seems to be more appropriate. A theoretical approach has been further adopted to clarify the difference between both models. We have calculated the theoretical $^{87}Sr/^{86}Sr$ expected in the case that Sr evaporation on Re filaments follows either a linear fractionation law (theoretically identical to the power law; e.g., Albarede, 1995; Dickin, 1995) or an exponential fractionation law.

If Sr evaporation followed a linear fractionation law, the measured $^{87}Sr/^{86}Sr$ at different $^{88}Sr/^{86}Sr$ would be:

$$^{87}Sr/^{86}Sr_{meas} = \frac{^{87}Sr/^{86}Sr_{true}}{1 + \varepsilon} \qquad (1)$$

where $^{87}Sr/^{86}Sr_{true}$ is the 'true' value of the ratio and ε is the mass discrimination factor per atomic mass unit (a.m.u):

$$\varepsilon = \frac{\left(\frac{^{88}Sr/^{86}Sr_{true}}{^{88}Sr/^{86}Sr_{meas}} - 1 \right)}{2} \qquad (2)$$

The result would be a $^{87}Sr/^{86}Sr_{lfl}$ constant and invariant with the degree of fractionation (solid line in Fig. 2b). If we applied wrongly an exponential fractionation law correction (see Appendix 1) to the $^{87}Sr/^{86}Sr_{meas}$, the $^{87}Sr/^{86}Sr_{efl}$ would result in a roughly inverse correlation with the degree of

fractionation, i.e. curve (1) in figure 2b. And this is not clearly the case for the measured exponential law corrected samples (open circles, Fig. 2b).

In contrast, if Sr evaporation followed an exponential fractionation law, the measured $^{87}Sr/^{86}Sr$ at different $^{88}Sr/^{86}Sr$ would be, following the equation of Thirlwall (1991) (see Appendix 1):

$$^{87}Sr/^{86}Sr_{meas} = {}^{87}Sr/^{86}Sr_{true} \left(\frac{^{88}Sr/^{86}Sr_{meas}}{^{88}Sr/^{86}Sr_{nat}} - 1 \right)^{0.503593} \quad (3)$$

where the value 0.503593 is given by the natural logarithm of the actual masses of the ^{88}Sr, ^{87}Sr, and ^{86}Sr isotopes, according to the relation:

TABLE 1
Sr fractionation law experiment on NIST SRM 987

SRM987	$^{88}Sr/^{86}Sr$	$^{87}Sr/^{86}Sr$ *lfl*	2 σ_m	$^{87}Sr/^{86}Sr$ *efl*	2 σ_m
batch n.					
I	8.3482	0.710255	± 8	0.710262	± 8
	8.3891	0.710264	± 11	0.710260	± 11
II	8.3593	0.710246	± 18	0.710252	± 18
	8.3452	0.710249	± 11	0.710258	± 11
III	8.4403	0.710272	± 14	0.710247	± 14
IV	8.3103	0.710231	± 8	0.710245	± 8
	8.3399	0.710248	± 10	0.710256	± 10
	8.3575	0.710239	± 10	0.710244	± 10
	8.3834	0.710248	± 11	0.710246	± 11
	8.4217	0.710263	± 9	0.710247	± 9
V	8.3406	0.710241	± 13	0.710247	± 13
	8.4140	0.710265	± 11	0.710248	± 11
VI	8.3179	0.710234	± 9	0.710247	± 9
	8.3493	0.710247	± 7	0.710254	± 7
	8.3673	0.710243	± 8	0.710246	± 8
	8.3848	0.710261	± 10	0.710258	± 10
	8.3860	0.710255	± 10	0.710252	± 10
	8.3905	0.710258	± 9	0.710253	± 9
	8.4121	0.710264	± 10	0.710250	± 10
	8.4125	0.710266	± 8	0.710253	± 8
	8.4459	0.710283	± 9	0.710255	± 9
VII	8.3119	0.710227	± 9	0.710242	± 9
			2 σ		*2 σ*
average		**0.710253**	± 28	**0.710251**	± 11

$^{88}Sr/^{86}Sr$: average measured value of each run. $^{87}Sr/^{86}Sr$ is presented corrected using both a linear (*lfl*) and an exponential (*efl*) fractionation law correction to $^{88}Sr/^{86}Sr = 8.375209$. Uncertainty in isotopic ratios refers to least significant digits and represents the internal precision (2σ_m). The average $^{87}Sr/^{86}Sr_{lfl}$ and $^{87}Sr/^{86}Sr_{efl}$ are reported at the bottom of the table along with the external precision (2σ). All measurements were performed in dynamic mode.

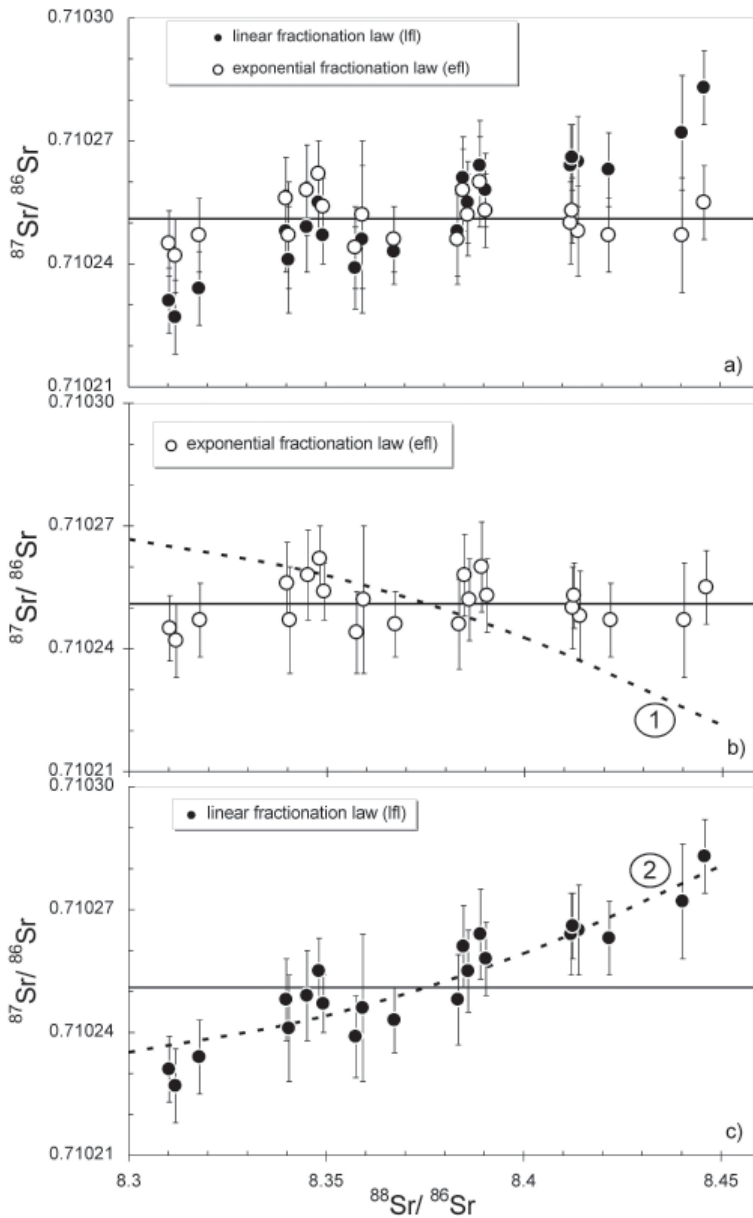Fig. 2 – $^{87}Sr/^{86}Sr$ vs. $^{88}Sr/^{86}Sr$ of replicate measurements of the NIST SRM 987 standard at different degree of fractionation (a), along with theoretical lines of $^{87}Sr/^{86}Sr$ raw data correction (b, c). Vertical bars represent the internal precision ($2\sigma_m$). The solid line in a, b, c refers to the mean $^{87}Sr/^{86}Sr$ value of our laboratory (0.710251, Table 5). Line 1 (b): theoretical $^{87}Sr/^{86}Sr$ variation if Sr evaporation followed a linear law and a wrong exponential fractionation law was applied to the raw data. Line 2 (c): theoretical $^{87}Sr/^{86}Sr$ variation if Sr evaporation followed an exponential law and a wrong linear fractionation law was applied to the raw data. It is clear that $^{87}Sr/^{86}Sr_{lfl}$ plot along line 2 (c), whilst $^{87}Sr/^{86}Sr_{efl}$ plot along the solid line rather than line 1 (b), demonstrating that the true fractionation behaviour of Sr evaporation can be approximated using an exponential law.

$$\frac{\ln(M_{87}/M_{86})}{\ln(M_{88}/M_{86})} = 0.503593 \qquad (4)$$

In this case, it would be the $^{87}Sr/^{86}Sr_{efl}$ constant and invariant with the degree of fractionation (solid line in Fig. 2c). And, if we applied wrongly a linear fractionation law correction to the $^{87}Sr/^{86}Sr_{meas}$, the $^{87}Sr/^{86}Sr_{lfl}$, this would result in a roughly positive correlation with the degree of fractionation, i.e. curve (2) in figure 2c. This is actually what we observe for the measured linear law corrected samples (closed circles, Fig. 2c).

The result provides evidence that the linear fractionation law is not adequate to explain the behaviour of Sr evaporation, and demonstrate that also using Re filaments, as with Ta filaments (Thirlwall, 1991), the true fractionation behaviour of Sr evaporation can be approximated using an exponential law.

The coincidence of the average $^{87}Sr/^{86}Sr_{lfl}$ and $^{87}Sr/^{86}Sr_{efl}$ (Table 1) is fortuitous and depends on the spread of $^{88}Sr/^{86}Sr$ (Fig. 2) around its stable natural value (i.e., 8.375209, according to the IUGS convention established by Steiger and Jager,

1977). The external reproducibility of $^{87}Sr/^{86}Sr_{lfl}$, however, is significantly worse than that of $^{87}Sr/^{86}Sr_{efl}$ (Table 1), and this is due to the inappropriate method adopted to correct for fractionation.

Static versus dynamic measurements

Two different methods and strategies can be used for Sr and Nd isotope measurements: *static* or *dynamic* mode.

The *static* mode consists of simultaneous measurements of all isotopes concerned using multiple collectors arranged in a fixed cup configuration, where each faraday cup collects always the same isotope (i.e., *main* configuration in Table 2). During the measurement the magnetic field remains static and the masses always hit the same detectors. In case of dynamic measurements the magnetic field is changed and shifts (jumps) different masses into different detectors. Static measurements have the advantage of reducing considerably acquisition time in comparison with the dynamic peak jumping technique, and avoids peak overlap problems during magnetic field jump. The static multi-collection technique has been

TABLE 2
Cup configuration schemes of Sr, Nd and Pb isotopic measurements

Sr isotopes configuration

Cup	L4	L3	L2	L1	C(Far)	H1	H2	H3	H4
jump 1				^{85}Rb	^{86}Sr	^{87}Sr	^{88}Sr		
jump 2 (Main)		^{84}Sr	^{85}Rb	^{86}Sr	^{87}Sr	^{88}Sr			
jump 3				^{86}Sr	^{87}Sr	^{88}Sr			

Nd isotopes configuration

Cup	L4	L3	L2	L1	C(Far)	H1	H2	H3	H4
jump 1				^{142}Nd	^{143}Nd	^{144}Nd	^{145}Nd	^{146}Nd	
jump 2 (Main)	^{140}Ce	^{141}Pr	^{142}Nd	^{143}Nd	^{144}Nd	^{145}Nd	^{146}Nd	^{147}Sm	^{148}Nd
jump 3				^{143}Nd	^{144}Nd	^{145}Nd	^{146}Nd	^{147}Sm	^{148}Nd

Pb isotopes configuration

Cup	L4	L3	L2	L1	C(Far)	H1	H2	H3	H4
Main				^{204}Pb	^{205}Tl	^{206}Pb	^{207}Pb	^{208}Pb	

generally limited to isotope dilution measurements, requiring lower precision than isotope composition measurements. This limitation is due to the uncertainty in Faraday cup efficiency and drift of electronics during the analysis. The Triton-Ti® is equipped with a *Virtual Amplifier*, which enables a variable connection between amplifiers and Faraday cups. This means that during a single analytical session each Faraday cup can be coupled to any of the 9 amplifiers, permitting a complete switching between amplifiers and cups. Thus the intensity of the signal in each Faraday cup can be measured by all the amplifiers. This procedure, along with the improvements in stability and low drift of the electronics, guarantees that the error in gain calibration and the error propagation into the calculated ratios are cancelled out. However, the *Virtual Amplifier* cannot correct for the different Faraday cup efficiency and its variation with time, since it depends on the cup itself including the material used and the geometry of the detector (see Wieser and Schwieters, 2005).

In contrast, the *dynamic* (or *multi-dynamic*) mode is a peak jumping procedure where a number of different cup configurations are employed for determining a single isotopic ratio (Table 2). This means that each isotope beam of the element to be measured, is monitored sequentially in different Faraday cups, and permits to cancel out both cup efficiency bias and drift of the electronics.

As an example we consider the measurement of Sr isotopes using the cup configuration reported in table 2. Combining the measurements from two different magnetic field position (jump 1-2 and jump 2-3, Table 2) it is possible to evaluate two independent $^{87}Sr/^{86}Sr_{double}$ defined as follows:

$$\left[\frac{^{87}Sr}{^{86}Sr}\right]_{1\text{-}2} = \sqrt{\left[\frac{^{87}Sr_{H1}}{^{86}Sr_C}\right]_1 \cdot \left[\frac{^{87}Sr_C}{^{87}Sr_{H1}}\right]_2 \cdot \left[\frac{^{88}Sr}{^{86}Sr}\right]_N} \quad (5)$$

$$\left[\frac{^{87}Sr}{^{86}Sr}\right]_{2\text{-}3} = \sqrt{\left[\frac{^{87}Sr_C}{^{86}Sr_{L1}}\right]_2 \cdot \left[\frac{^{87}Sr_{L1}}{^{88}Sr_C}\right]_3 \cdot \left[\frac{^{88}Sr}{^{86}Sr}\right]_N} \quad (6)$$

where the numbers outside the parentheses are relative to the three different magnetic field positions, the subscript of each isotope refers to the cup on which it is measured and $[^{88}Sr/^{86}Sr]_N$ is the natural ratio (i.e., 8.375209).

Since the connection between cups and amplifiers is kept fixed, the subscript referring to the different cup position represents the sum of the effect of cups and amplifiers efficiencies. Equations (5) and (6) clearly demonstrate that adopting this procedure allows to cancel out all cup biases and electronic drift from measured isotopic ratios.

Such a calculation, however, implies a linear correction for mass fractionation, and therefore the two $^{87}Sr/^{86}Sr_{double}$ need to be uncorrected for linear fractionation dividing by the factor $1+\varepsilon$ (see Appendix 1), and then corrected again using the appropriate *exponential fractionation law* (see the above paragraph) and the $^{88}Sr/^{86}Sr$ measured on the *main* magnetic field position (jump 2, Table 2).

The two $^{87}Sr/^{86}Sr_{double}$ exponential law corrected are geometrically averaged to obtain a single $^{87}Sr/^{86}Sr_{triple}$ value. A similar procedure is adopted for Nd isotope measurement (Table 2); in this case the $^{143}Nd/^{144}Nd_{triple}$ linearly corrected for fractionation is obtained as follows:

$$\left[\frac{^{143}Nd}{^{144}Nd}\right]_{Triple} =$$

$$\sqrt{\left[\frac{^{143}Nd_C}{^{144}Nd_{H1}}\right]_1 \cdot \left[\frac{^{143}Nd_{L1}}{^{144}Nd_C}\right]_2 \cdot \left[\frac{^{146}Nd_{H1}}{^{144}Nd_{L1}}\right]_3 \cdot \left[\frac{^{144}Nd}{^{146}Nd}\right]_N} \quad (7)$$

As with the Sr isotope dynamic measurement, this ratio cancels out the relative bias between the different cups and amplifiers, but in this case the normalisation to the natural $^{144}Nd/^{146}Nd$ (0.7219) results in an incomplete linear correction. In equations (5) and (6) all the measured isotope ratios have 1 a.m.u. difference, producing the reciprocal elimination of the linear correction factors and resulting in an automatic linear correction of the ratios. In contrast, the first two isotope ratios of equation (7) have a 1 a.m.u. difference, whilst the third ratio has a 2 a.m.u. difference; in this case, the linear correction need to be not reciprocally cancelled unless considering $(1+\varepsilon)^2 \approx (1+2\varepsilon)$. Therefore the factor $(1+2\varepsilon)/(1+\varepsilon)^2$ is added to equation (7) to obtain a $^{143}Nd/^{144}Nd_{triple}$ linearly corrected for fractionation, then the isotopic ratio is uncorrected for linear fractionation dividing by the factor $(1+\varepsilon)$, and eventually corrected again using the appropriate *exponential fractionation law* (see Appendix 1). The cup configuration of Nd isotope measurement enables also to calculate a $^{145}Nd/^{144}Nd_{triple}$ and a $^{142}Nd/^{144}Nd_{double}$.

As outlined above the multi-dynamic method has the great advantage to cancel out all the possible differences in the efficiencies of both the Faraday cups and the amplifiers. The main disadvantage of the *peak jumping* procedure has to do with the longer analysis-time and the necessity of an optimal cup alignment to measure different masses in the same cup after each jump. The latter problem is solved in the ThermoFinnigan Triton-Ti® by the *Zoom Optics*, a device consisting of two sets of electromagnetic lenses placed before and after the magnet, which enables to slightly change the dispersion and the focus of the beam to obtain a perfect peak overlapping in the different jumps.

In order to choose the most suitable method for our aims we performed several run in both static and dynamic methods, evaluating many different parameters such as internal and external precision, concordance of the measured ratio with the recommended value, time spent, amount of sample required and beam intensity. As stated above, the main advantages of the *static* and *dynamic* mode are the short measuring time and the cross calibration of the cup efficiency bias, respectively. The latter in particular cannot be corrected with neither the "gain calibration" nor the amplifier rotation (*Virtual Amplifier*), but requires a complex Faraday cup efficiency (FCE) calibration procedure (Makishima and Nakamura, 1991), which consists in replicate measurements of the same isotopic ratio (e.g., $^{143}Nd/^{144}Nd$) with different cup configurations. Being the FCE calibration an extremely time-consuming process,

which needs to be performed frequently (e.g., once a month) to ensure the correction of possible FCE drifts, the main advantage of the *static* measurements results strongly weakened. To test the possibility of performing static measurements without FCE calibration we have measured replicates of NIST SRM 987 with 9 blocks of 180 cycles (8 s integration time and amplifiers rotation) and ~5V of ^{88}Sr beam for a total measuring time of 30 minutes. The resulting mean value of $^{87}Sr/^{86}Sr$ has been 0.710264 ± 15 (2σ, n = 97, internal precision ≥ 10ppm), which is slightly higher than the recommended value (0.710248 ± 11, Thirlwall, 1991), and worse in term of both internal and external precision with respect to the dynamic value (see later discussion and Table 3). The results confirm the necessity of the FCE calibration for static measurements to obtain data with comparable accuracy and precision with respect to those measured in dynamic mode. It has to be highlighted that the higher the signal the lower the instrumental error (i.e., internal precision); thus it would be possible to increase our performance simply running samples at higher intensity. However, the prolonged use of high intensity beams would also produce a more rapid deterioration of the Faraday cups, enhancing the possibility of the time-dependent cup deterioration and thus requiring more frequent FCE calibration. According to these considerations we decided to perform Sr and Nd isotope measurement using the dynamic mode. Obviously, static measurements of Sr and Nd samples can be performed after the appropriate FCE calibration in the case of

TABLE 3
Mean values and external precision of Sr isotope ratios of NIST SRM 987

Sr standard		$^{87}Sr/^{86}Sr$ triple	2σ	$^{84}Sr/^{86}Sr$ static	2σ	n.
SRM 987	Firenze	0.710251	± 11	0.056491	± 6	162
	Thirlwall (1991)	0.710248	± 11 (427)	0.056492	± 16 (73)	

Sr isotopes have been measured in dynamic mode. The mass bias correction is performed with an exponential fractionation law (Appendix 1) using the natural value $^{88}Sr/^{86}Sr$ = 8.375209, as described in the text. Uncertainty in isotopic ratios refers to least significant digits and represents the external precision (2σ). n: number of measurements; The number of replicates of literature data, when available, is reported in brackets next to the external precision.

extremely low size samples (i.e. micro-drilled samples) to reduce measuring times.

The *static* mode, in contrast, has been used to perform Pb isotope, since lead has not a pair of stable isotopes to properly correct for mass fractionation and hence the internal precision of Pb measurements (ca. 80 ppm) is lower than that of Sr and Nd. Therefore, in this case the *peak jumping* procedure cannot improve significantly the final result, whilst the *static mode* enables short acquisition times without affecting much the precision of the measurement.

Results on certified reference materials

Sr isotopes

We have extensively carried out a large number of Sr isotope measurements on the NIST SRM 987. We loaded on single Re filament about 100-150 ng of reference material in nitrate form with a Ta activator and H_3PO_4, and with a beam intensity of ~ 4 V for ^{88}Sr.

Sr isotope ratios were measured in *dynamic* mode using the cup configuration scheme reported in table 2. The different isotope ratios were measured using 120 sets of cycles, taken in 6 blocks, each consisting of 20 cycles with 8 seconds integration time. An idle time of 3 seconds was set before the start of the collection after each jump, to eliminate possible memory effect due to the decay of the signal in the faraday cups.

The instrumental mass bias has been corrected *off line* using the $^{88}Sr/^{86}Sr$ ratio measured on the *main* configuration (jump 2; Table 2). The measured and the natural $^{88}Sr/^{86}Sr$ ($^{88}Sr/^{86}Sr_N$ = 8.375209) have been used both to calculate the mass discrimination factor (ε) and to subsequently apply the correction through the *exponential fractionation law* (see Appendix 1).

^{85}Rb has been set onto the L2 collector to monitor the ^{87}Rb contribution (i.e., isobaric interference), if any, to the reading of mass 87 using the natural $^{87}Rb/^{85}Rb$ (i.e., 0.386).

The analysis time, including lens focusing, peak centering, and baseline measurement (32 s) before and after each block, was ca. 75 minutes; the warm-up procedure was ca. 35 minutes. The results are reported in table 3 and shown in figure 3. The mean $^{87}Sr/^{86}Sr_{triple}$ value has been 0.710251 ± 11 (2σ, n = 162), which is well within the recommended value ($^{87}Sr/^{86}Sr$ = 0.710248 ± 11; Thirlwall, 1991). The internal precision (2σ$_m$) of $^{87}Sr/^{86}Sr_{triple}$ has been typically ≤10 ppm.
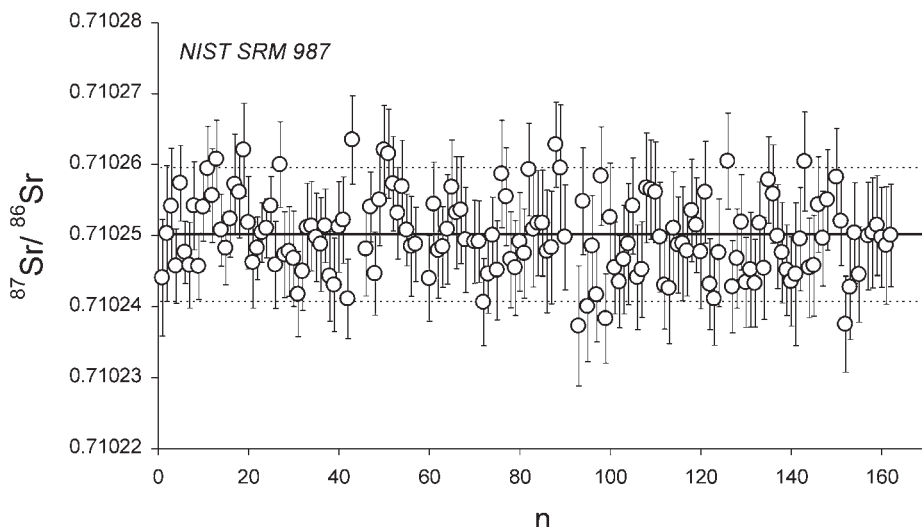

Fig. 3 – $^{87}Sr/^{86}Sr_{triple}$ of replicate measurements of the NIST SRM 987 standard with average (solid line) and external precision (2σ, dashed lines). Vertical bars represent the internal precision (2σ$_m$).

Nd isotopes

Nd isotope measurements have been performed on international (La Jolla) and internal (NdFi) reference materials. The NdFi is the Nd isotope standard of our laboratory, made from commercially available Nd_2O_3 (Neodymium (III) Merck®; purity > 99%). We loaded on double Re filaments about 90-150 ng of reference material in nitrate form with H_3PO_4, with a beam intensity of ~ 1.5-2.0 V for ^{144}Nd.

Nd isotope ratios were also measured in *dynamic* mode using the cup configuration scheme reported in table 2. The different isotopic ratios were measured using 110 cycles, taken in 10 blocks, each consisting of 11 cycles with 8 seconds integration time. An idle time of 3 seconds was also set before the start of the collection after each jump, to eliminate possible memory effect due to the decay of the signal in the faraday cups.

The instrumental mass bias has been corrected *off line* using the $^{146}Nd/^{144}Nd$ ratio measured on the *main* configuration (jump 2; Table 2). The measured and the natural $^{146}Nd/^{144}Nd$ (i.e., 0.7219) have been used both to calculate the mass discrimination factor (ε) and to subsequently apply the correction through the *exponential fractionation law* (see Appendix 1).

^{140}Ce and ^{147}Sm have been set onto the L4 and H3 collectors respectively (Table 2), to monitor and correct for the ^{142}Ce and ^{144}Sm contributions to the reading of masses 142 and 144.

The analysis time, including lens focusing, peak centering, and baseline measurement (32 s) before and after each group of three blocks, was ca. 60 minutes; the warm-up procedure was ca. 40 minutes. The results for both La Jolla and NdFi reference material samples are reported in table 4 and shown in figure 4. The mean $^{143}Nd/^{144}Nd_{triple}$ value of La Jolla reference material has been 0.511845 ± 7 (2σ, n = 42), which is comparable to the recommended value ($^{143}Nd/^{144}Nd$ = 0.511856 ± 7; Thirlwall, 1991). The mean $^{143}Nd/^{144}Nd_{triple}$ value of NdFi reference material has been 0.511465 ± 6 (2σ, n = 51). The internal precision ($2\sigma_m$) of $^{143}Nd/^{144}Nd_{triple}$ has been typically ≤10 ppm.

The external precision of the stable Nd isotope ratios (Table 4) is excellent for the two standards measured in our laboratory, and the absolute values are identical within error of the reference values reported in the literature (Table 4). Considering

TABLE 4

Mean values and external precision of Nd standards

Nd standards	Laboratory-ref.	$^{142}Nd/^{144}Nd$ double	2σ	$^{143}Nd/^{144}Nd$ triple	2σ	$^{145}Nd/^{144}Nd$ double	2σ	$^{148}Nd/^{144}Nd$ static	2σ	n
La Jolla	Firenze	1.141841	± 30	0.511845	± 7	0.348399	± 5	0.241578	± 11	42
	Thirlwall (1991)			0.511856	± 7	0.348410	± 12			24
	VU. Amsterdam			0.511852	± 7					44
Nd Fi	Firenze	1.141841	± 20	0.511465	± 6	0.348401	± 5	0.241577	± 10	51
BCR 1-USGS	Wasserburg et al. (1981)	1.141876	± 9 ($?2\sigma_m$)	0.512646	± 9 ($?2\sigma_m$)	0.348415	± 6 ($?2\sigma_m$)	0.214587	± 6 ($?2\sigma_m$)	

Nd isotopes have been measured in dynamic mode and are corrected for mass fractionation as described in the text, normalising to the natural value $^{146}Nd/^{144}Nd$ = 0.7219 according to an exponential fractionation law (Appendix 1). Uncertainty in isotopic ratios refers to least significant digits and represents the external precision (2σ). n: number of measurements. La Jolla analyses performed at the Vrije Universiteit (authors' unpublished data) are reported as an inter-laboratory term of comparison. NdFi is the internal standard of our laboratory (see text). BCR1-USGS is a natural standard here reported as reference for Nd stable isotope ratios (Wasserburg et al., 1981).
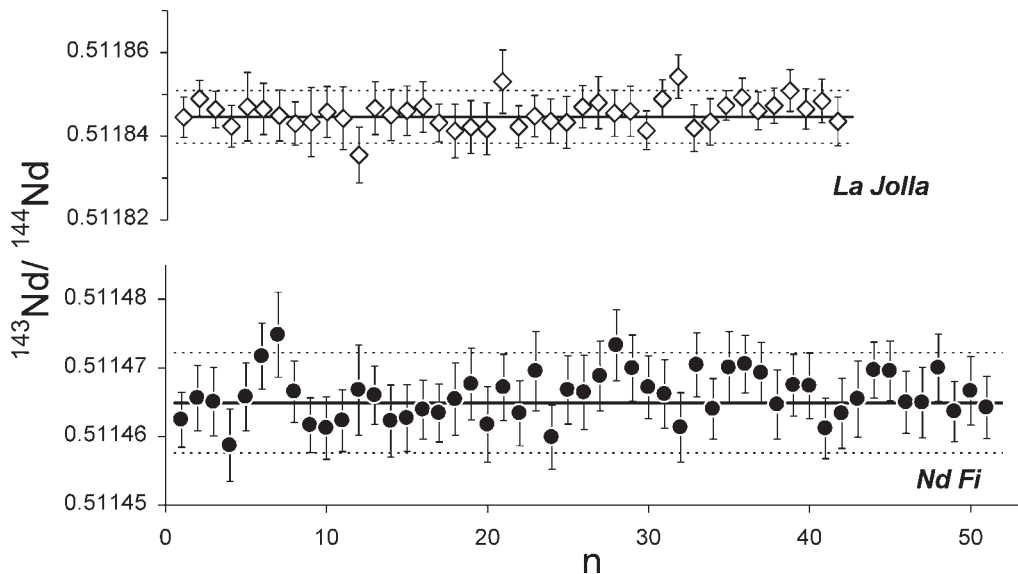
Fig. 4 – $^{143}Nd/^{144}Nd_{triple}$ of replicate measurements of the La Jolla and NdFi standards. Solid and dashed lines of each standard represent the average and the external precision (2σ), respectively. Vertical bars represent the internal precision (2σ_m). NdFi is the internal Nd isotope standard of our laboratory (see text).

the NdFi internal reference material has not been purified, and then contains some Ce impurities, the identical $^{142}Nd/^{144}Nd$ value obtained for the NdFi and LaJolla reference materials confirms the accuracy of our interference correction.

Pb isotopes

Pb isotope measurements have been performed on the NIST SRM981 standard reference material. About 50ng of reference material were loaded onto single zone-refined Re filament in nitrate form along with 0.5μl of silica gel (Yokoyama et al., 2001) and 1μl of H_3PO_4, obtaining a beam intensity of 1.5-2 V ^{208}Pb at a temperature of ca. 1300°C.

Pb isotope ratios were measured in *static mode*, using the cup configuration scheme reported in table 2. The different isotope ratios were measured using 180 cycles, taken in 6 blocks each consisting of 30 cycles with 4 seconds integration time. The analysis time, including lens focusing, peak centering, and baseline measurement (32 s) before

and after each block, was ca. 20 minutes; the warm-up procedure was ca. 25 minutes.

The measured raw values for the NIST SRM981 reference material are reported in table 5 and shown in figure 5 along with the theoretical linear fractionation line calculated from the reference values (Thirlwall, 2000). The mean raw values for the NIST SRM981 are: $^{206}Pb/^{204}Pb$ = 16.889 ± 6 (2σ, n =11), $^{207}Pb/^{204}Pb$ = (15.427± 9 (2σ, n =11), and $^{208}Pb/^{204}Pb$ = 36.497 ± 28 (2σ, n =11) (Table 5). The internal precision (2σ_m) of Pb isotopes ratioed to ^{204}Pb is typically <80 ppm.

The measured raw values of $^{208}Pb/^{207}Pb$, $^{208}Pb/^{206}Pb$, and $^{207}Pb/^{206}Pb$ have been used to calculate the mean *mass discrimination factor* (ε = 1.39 ± 20 ‰ per a.m.u., 2σ n=11), according to the *linear fractionation law* correction (eq. A-3 in Appendix 1). This average value has been subsequently used to correct measurements of unknown samples, along with the Pb isotopes of the NIST SRM981 ratioed to ^{204}Pb. The linear corrected ratios (Table 5) are identical, within error, to the recommended values of the NIST SRM981 (Thirlwall, 2000; Todt et al., 1996; Table 5).
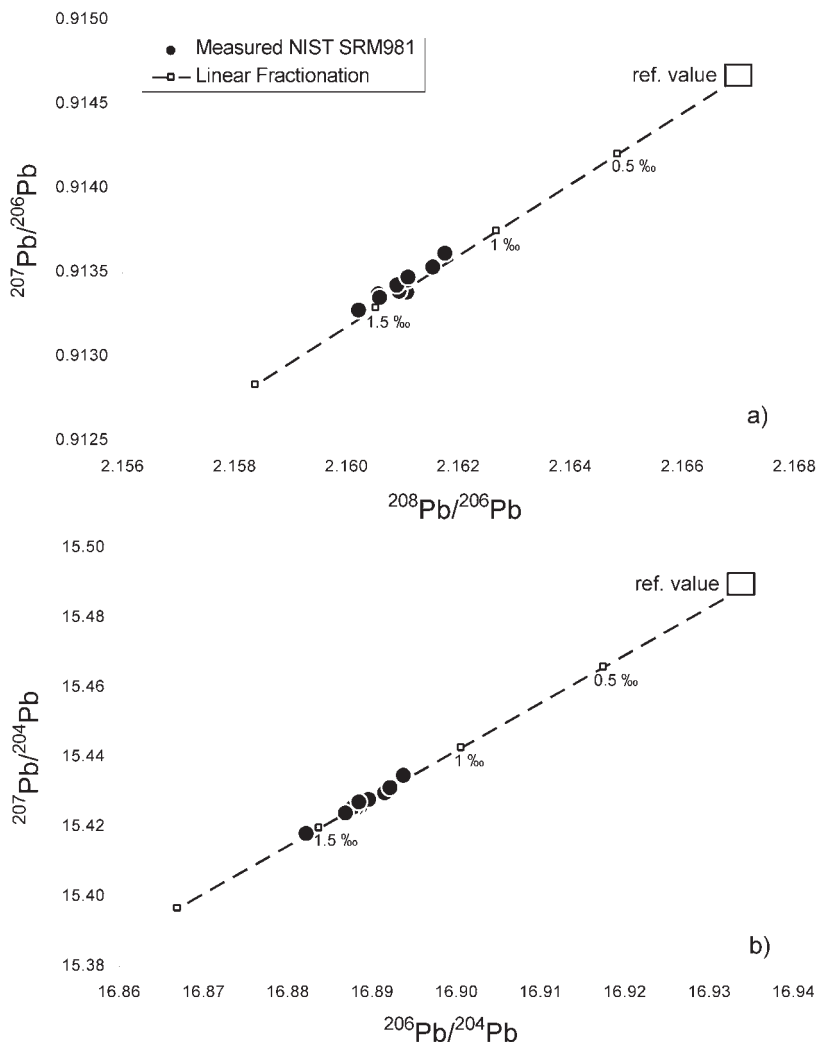
Fig. 5 – $^{207}Pb/^{206}Pb$ *vs.* $^{208}Pb/^{206}Pb$ (a) $^{207}Pb/^{204}Pb$ *vs.* $^{206}Pb/^{204}Pb$ (b) of replicate measurements of the NIST SRM 981 standard along with theoretical (dashed) lines of isotopic fractionation calculated with the linear fractionation law (see Appendix 1). Starting reference values are from Thirlwall (2000) and Todt et al. (1996). The numbers on the theoretical lines represent the different values of the *mass discrimination* factor (ε).

FINAL REMARKS

Modern isotope geology is a rapidly expanding discipline that has a wide-range application in all of the Earth and Planetary Sciences, from solar system processes to environmental geosciences, through mantle and crust processes and evolution, radiometric dating, timing and flux history of near surface reservoirs.

The high-quality procedures set up in our laboratory for determining Sr, Nd, and Pb isotopes on geologic materials are apt to perform advanced and innovative research on the aforementioned geologic issues. Our experiments led to perform

TABLE 5
Mean values and external precision of NIST SRM 981 Pb isotope standard

			$^{206}Pb/^{204}Pb$	2σ	$^{207}Pb/^{204}Pb$	2σ	$^{208}Pb/^{204}Pb$	2σ	n.
SRM 981	Firenze	raw values	16.889	± 6	15.427	± 9	36.497	± 28	11
		lin. corrected	16.936	± 6	15.491	± 9	36.699	± 28	
	Thirlwall (2000)		16.934	± 3	15.489	± 3	36.697	± 7	32

			$^{207}Pb/^{206}Pb$	2σ	$^{208}Pb/^{206}Pb$	2σ	$^{208}Pb/^{207}Pb$	2σ
SRM 981	Firenze	raw values	0.91343	± 18	2.1610	± 9	2.3658	± 5	11
	Thirlwall (2000)		0.91466	± 12	2.167		2.3692	± 3	32
	ε_m		*0.00135*	*± 20*	*0.00139*	*± 20*	*0.00143*	*± 20*

Pb isotopes have been measured in static mode; *raw values* are not corrected for mass bias; *lin. corrected* values are corrected with a linear fractionation law (Appendix 1) using the mean calculated *mass discrimination factor* ($\varepsilon = 1.39$ ‰ ± 10 per a.m.u); the three values of ε reported in the table are calculated separately for the $^{208}Pb/^{207}Pb$, $^{208}Pb/^{206}Pb$, and $^{207}Pb/^{206}Pb$ ratios respectively. The reference values used for calculating ε are also reported in the table and are taken from Thirlwall (2000) except for $^{208}Pb/^{206}Pb$ which is from Todt et al. (1996). Uncertainty in isotopic ratios refers to least significant digits and represents the external precision (2σ). n: number of measurements.

high precision data using a dynamic mode for Sr and Nd measurements and correcting for mass bias using an exponential fractionation law. The choice to perform measurements in dynamic rather than static mode leads to a more time-consuming analytical schedule but allows the obtainment of more precise and accurate isotopic determinations. This permits to obtain meaningful data also on geologic material having very small isotopic differences (e.g., ca. 15 ppm for Sr and Nd isotopes).

Pb isotope measurements have been performed in static mode and corrected for mass bias using a linear fractionation law, since the advantages of the dynamic procedure are not significant with the lower precision obtainable for these isotopic ratios.

The application on natural samples from different magmatic associations, of the described instrumental procedures, has provided important data to constrain magmatic processes.

The determination of Sr isotope ratios in volcanic sequences of active, continuously erupting, volcanoes, in which small isotopic differences are observed among the different products emitted with

time, has been used to investigate the dynamics of active volcanoes (e.g., Stromboli) and to establish open vs. closed system magmatic evolution (e.g., Francalanci et al., 1999, 2004). The determination of accurate and precise isotopic data on different phases of each single rock has permitted also to define isotopic equilibrium among minerals and glasses (e.g., Francalanci et al., 2004; 2005).

Other applications of our isotopic data have been aimed to investigate evolutionary processes in complex magmatic systems (Petrone et al., 2006) and the heterogeneity of the mantle sources in different tectonic settings. Particular interest has been devoted to constrain the role of fluids vs. melts in metasomatic processes (Orozco-Esquivel et al., 2006, Avanzinelli et al., in prep.) and to determine the time-integrated isotopic compositions of mantle sources (e.g., Melluso et al., 2004, 2005). Moreover, Sr, Nd and Pb isotopes have been utilised as tracers of natural processes in running ground and thermal waters (Nisi, 2005).

The ambitious perspective is, thus, to give rise to an efficient radiogenic isotope geology laboratory that will produce up-to-date research covering most of the potential applications in

Earth Sciences fields. In this context, we are also establishing in-situ micro-sample (<1 mg) isotopic analyses and we are planning to set up the analytical and instrumental procedures for the measurements of U-series disequilibria, thanks to the RPQ-equipped Secondary Electron Multiplier (SEM) device described earlier. This will enable our laboratory to further enlarge the spectrum of possible applications: for example, the short-lived isotopes of the Uranium decay series are being increasingly used since the last two decades in examining short-range processes, from dating of Quaternary-age sedimentary rocks to assessing the dynamics of mantle melting and rate of melt production and crustal growth.

APPENDIX 1 – MASS FRACTIONATION CORRECTION IN ISOTOPIC RATIO MEASUREMENTS

Three *fractionation laws* are commonly used to correct empirically for isotopic fractionation (*linear*, *power* and *exponential law*). The *linear* and *power law* are derived from the theoretical *Rayleigh distillation law* using different assumptions (see Albarede, 1995, for a thorough discussion). The *Exponential Law*, firstly introduced by Russel et al (1978) to account for the behaviour of "light"

Ca, represents a different theoretical approach to account for isotopic fractionation correction.

Following Wasserburg et al. (1981) and Lee et al. (2001) notation, let be:

- R_{ij} the isotopic ratio of isotopes *i* and *j* with masses *mi* and *mj*
- R^N_{uv} an isotopic reference value of a selected pair of isotopes *u* and *v*

For the *linear fractionation law* we use the following equation for the corrected ratio:

$$R^C_{ij} = R^M_{ij} (1 + \varepsilon \cdot \Delta m_{ij}) \tag{A1}$$

where R^C is the corrected ratio, R^M the measured one, Δm_{ij} is the difference between the nominal masses of the two isotopes *i* and *j,* and ε represents the *mass discrimination factor ε_{LIN} (u,v)* and is determined by

$$\varepsilon_{LIN} (u, v) = \frac{\left[\dfrac{R^N_{uv}}{R^M_{uv}} - 1 \right]}{\Delta m_{uv}} \tag{A2}$$

in the case of Sr isotopes the two equation can be written as follows:

$$\varepsilon_{LIN} (^{88}Sr, ^{86}Sr) = \frac{1}{2} \cdot \left[\frac{8.375209}{\frac{^{88}Sr}{^{86}Sr} \, meas} - 1 \right] \tag{A3}$$

and thus the ratio corrected with the linear fractionation law (*lfl*) is

$$\frac{^{87}Sr}{^{86}Sr} \, lfl = \frac{^{87}Sr^M}{^{86}Sr} \cdot (1 + \varepsilon_{LIN}) \tag{A4}$$

The *Power Law* is another method to account for mass fractionation. The corrected ratio is given by

$$R^C_{ij} = R^M_{ij} [1 + \alpha_P]^{\Delta m_{ij}} \tag{A5}$$

where the *mass discrimination factor $\alpha_p(u,v)$* is

$$\alpha_P (u, v) = \left[\frac{R^N_{uv}}{R^M_{uv}} \right]^{\frac{1}{\Delta m_{uv}}} - 1 \tag{A6}$$

the masses used in this equation are nominal and the equation for Sr isotopes can be written as

$$\alpha_P \left({}^{88}Sr, {}^{86}Sr \right) = \left[\frac{8.375209}{\frac{{}^{88}Sr^M}{{}^{86}Sr}} \right]^{\frac{1}{2}} - 1 \qquad (A7)$$

and

$$\frac{{}^{87}Sr^C}{{}^{86}Sr} = \frac{{}^{87}Sr^M}{{}^{86}Sr} [1 + \alpha_P] \qquad (A8)$$

It is important to note that both the *linear* and *power* law corrections consider the difference between masses (Δm), hence, for instance, $\Delta_{86,88} = \Delta_{146,144} = 2$.

In the *Exponential Law* the corrected ratio is given by

$$R^C{}_{ij} = R^M{}_{ij} \cdot \left(\frac{m_i}{m_j} \right)^{\beta} \qquad (A9)$$

where $m_{i,j}$ are the "real" mass values of the different isotopes i and j; β the *exponential mass discrimination factor* defined as

$$\beta = \frac{\ln \left[\frac{R^N{}_{uv}}{R^M{}_{uv}} \right]}{\ln \left[\frac{m_u}{m_v} \right]} \qquad (A10)$$

For Sr isotopes the two equations can be written either as

$$\beta = \frac{\ln \left[\frac{8.375209}{\frac{{}^{88}Sr^M}{{}^{86}Sr}} \right]}{\ln \left[\frac{87.9056}{85.9093} \right]} \qquad (A11)$$

and

$$\frac{{}^{87}Sr}{{}^{86}Sr} \, efl = \frac{{}^{87}Sr^M}{{}^{86}Sr} \cdot \left(\frac{86.9088}{85.9093} \right)^{\beta} \qquad (A12)$$

or, following Thirlwall (1991):

$$\left[\frac{\frac{{}^{86}Sr}{{}^{86}Sr}}{\frac{{}^{87}Sr^M}{{}^{86}Sr}} \right]^{C \ln\left(\frac{m_{88}}{m_{86}} \right)} = \left[\frac{\frac{{}^{86}Sr}{{}^{86}Sr}}{\frac{{}^{88}Sr^M}{{}^{86}Sr}} \right]^{\ln\left(\frac{m_{87}}{m_{86}} \right)} \qquad (A13)$$

and

$$\frac{{}^{87}Sr}{{}^{86}Sr} \, efl = \frac{{}^{87}Sr^M}{{}^{86}Sr} \cdot \left[\frac{8.375209}{\frac{{}^{88}Sr^M}{{}^{86}Sr}} \right]^{\frac{\ln\left(\frac{m_{87}}{m_{88}} \right)}{\ln\left(\frac{m_{88}}{m_{86}} \right)}} \qquad (A14)$$

These two different expressions of the *exponential fractionation law* (*efl*) are linked by the mathematical relation

$$a^{\ln b} = b^{\ln a} \qquad (A15)$$

The main difference of this law, with respect to the previous two, is that the *exponential law* takes into account the size of the masses of the different isotopes instead of their difference; that is, referring to the previous example, $\ln\left(\frac{m_{86}}{m_{88}} \right) \neq \ln\left(\frac{m_{144}}{m_{146}} \right)$.

Recently, some authors demonstrated that the *exponential fractionation law* (*efl*) correction is the best adequate for isotopic ratio corrections in both Thermal Ionisation (Thirlwall, 1991) and Plasma source equipments (Luais et al., 1997; Marechal et al., 1999).

REFERENCES

Albarede F. (1995) – *Introduction to geochemical modeling*. Cambridge University Press, Cambridge, 543 pp.

Avanzinelli R., Elliott T., Tommasini S. and Conticelli S. (2005) – *U-Th disequilibria and Sr-Nd isotopes in Central-Southern Italy: evidences for subduction-related fluids and recycled sedimentary melts in the genesis of recent Italian potassic and ultrapotassic magmas*. In preparation.

Crock J.G, Lichte F.E. and Wildeman T.R. (1984) – *The group separation of the rare-earth elements and yttrium from geological materials by cation-exchange chromatography*. Chem. Geol. **45**, 149-163.

Croudace I.W. (1980) – *A possible error source in silicate wet-chemistry caused by insolubile fluorindes*. Chemical Geology **31**, 153-155.

Curie M.S. (1898) – *Rayons emis part les composes de l'uranium et du thorium*. Comptes Rendus de Seances de l'Academie de Sciences, **126**, 1101-1103.

DENIEL C. and PIN C. (2001) – *Single-stage method for the simultaneous isolation of lead and strontium from silicate samples for isotopic measurements.* Anal. Chim. Acta, **426**, 95-103.

DICKIN A.P. (1995) – *Radiogenic Isotope Geology.* Cambridge University Press, Cambridge, 452 p.

EBERHART A., DELWICHE R. and GEISS Z. (1964) – *Isotopic effects in single filament thermal ion sources.* Z. Natur. **19**a, 736-740.

FAURE G. (1986) – *Principles of Isotope Geology.* Wiley, New York, 589 p.

FRANCALANCI L., DAVIES G.R., LUSTENMHOWER W., MASON P., TOMMASINI S. and CONTICELLI S. (2005) – *In Situ Sr-Isotope Microanalysis Evidence of Old Crystal Re-Cycling and Multiple Magma Reservoirs in the Plumbing System of the Present Day Activity at Stromboli, South Italy.* J. Petrol. **46**, 1997-2021.

FRANCALANCI L., TOMMASINI S., CONTICELLI S., and DAVIES G.R. (1999) – *Sr isotope evidence for short magma residence time for the 20th century activity at Stromboli volcano, Italy.* Earth Planet. Sci. Lett., **167**, 61-69.

FRANCALANCI L., TOMMASINI S. and CONTICELLI S. (2004) – *The volcanic activity of Stromboli in the 1906-1998 AD period: mineralogical, geochemical and isotope data relevant to the understanding of the plumbing system.* J. Volcanol. Geotherm. Res., **131**, 179-211.

HABFAST K. (1983) – *Fractionation in the thermal ionisation source.* International Journal of Mass Spectrometry Ion Physic, **51**, 165-189

LEE C.-T., YIN Q.-Z. and LEE T.-C. (2001) – *An internal normalization technique for unmixing total-spiked mixtures with application to MC-ICP-MS.* Comp. Geosci., **27**, 577-581.

LUAIS B., TELOUK P. and ALBAREDE F. (1997) – *Precise and accurate neodymium isotopic measurements by plasma-source mass spectrometry.* Geochim. Cosmochim. Acta, **61**, 4847-4854.

MAKISHIMA A. and NAKAMURA E. (1991) – *Calibration of Faraday cup efficiency in multicollector mass spectrometer.* Chem. Geol., **94**, 105-110.

MARECHAL C.N., TELOUK P. and ALBAREDE F. (1999) – *Precise analyses of copper and zinc isotopic compositions by plasma-source mass spectrometry.* Chem. Geol., **156**, 251-273.

MELLUSO L., CENSI P., PERINI G., VANCONCELOS L., MORRA V., GUERRIERO F. and BENNIO L. (2004) – *Chemical and isotopic (C, O, Sr, Nd) characteristics of the Xiluvo carbonatite (central- western Mozambique).* Mineral. Petrol. **80**, 201-213.

MELLUSO L., MORRA V., BROTZU P., D'AMELIO F., TOMMASINI S., FRANCIOSI L., RENNA M.R. and DUNCAN R.A. (2005) – *Geochronology and petrogenesis of the Cretaceous Antampombato-Ambatovy complex and associated dyke swarm, Madagascar.* J. Petrol. **46**, 1963-1996.

NIER A.O. (1940) – *A Mass Spectrometer for routine isotope abundance measurements.* Review of Scientific Instruments, **11**, 212-216.

NIER A.O. (1947) – *A Mass Spectrometer for isotope and gas analysis.* Review of Scientific Instruments, **18**, 398-411.

NISI B. (2005) – *Geochimica ed isotopi ambientali nelle acque di scorrimento superficiale della Valle dell'Arno: inquinamento antropico e naturale.* Unpublished PhD Thesis, University of Florence, p. 320.

OROZCO-ESQUIVEL M.T., PETRONE C.M., TAGAMI T., FERRARI L. and MANETTI P. (2006) – *Geochemical and isotopic variability controlled by slab detachment in a subduction zone with variable dip: the Eastern Trans-Mexican Volcanic Belt.* Submitted to Lithos.

PETRONE C.M., FRANCALANCI L., FERRARI L., SCHAAF P. and CONTICELLI S. (2005) – *The San Pedro-Cerro Grande Volcanic Complex (Nayarit, Mexico): inferences on volcanology and magma evolution.* In Siebe C., Aguirre-Dìaz G., Luis-Macías J. (eds), "Neogene-Quaternary continental margin volcanism: a perspective from Mexico". GSA Special Paper, in press.

RICHARD P., SHIMIZU N. and ALLEGRE C. (1976) – *$^{143}Nd/^{144}Nd$, a natural tracer: an application to oceanic basalts.* Earth Planet. Sci. Lett. **31**, 269-278.

RUSSEL W.A., PAPANASTASSIOU D.A. and TOMBRELLO T.A. (1978) – *Ca isotope fractionation on the Earth and other solar system materials.* Geochim. Cosmochim. Acta **42**, 1075-1090.

STEIGER R.H. and JÄGER E. (1977) – *Subcommission on geochronology: convention on the use of decay constants in geo- and cosmochronology.* Earth Planet. Sci. Lett., **36**, 359-362.

THIRLWALL M.F. (1991) – *Long-term reproducibility of multicollector Sr and Nd isotope ratio analysis.* Chem. Geol., **94**, 85-104.

THIRLWALL M.F. (2000) – *Inter-laboratory and other errors in Pb isotope analyses investigated using a $^{207}Pb-^{204}Pb$ double spike.* Chem. Geol., **163**, 299-322.

TODT W., CLIFF R.A., HENSER A. and HOFFMANN A.W.

(1996) – *Evaluation of a ^{202}Pb-^{205}Pb double spike for high precision lead isotope analysis*. Geophys. Monogr. **95**, 429-437

Wasserburg G.J., Jacobsen S.B., DePaolo D.J., McCulloch M.T. and Wen T. (1981) – *Precise determination of Sm/Nd ratios, Sm and Nd isotopic abundances in standard solutions*. Geochim. Cosmochim. Acta, **45**, 2311-2323.

Yokoyama T., Makishima A. and Nakamura E. (2001) – Precise analysis of $^{234}U/^{238}U$ ratio using UO_2^+ ion with thermal ionization mass spectrometry for natural samples. Chem. Geol., **181**, 1-12.

Wieser M.E. and Schwieters J.B. (2005) – *The development of multiple collector mass spectrometry for isotope ratio measurements*. Int. J. of Mass Spectrometry, **242** (2-3), 97-115.

The reference list is arranged in alphabetical order following the surname of the first authors. In the case of multiple authors they will be arranged following the further authors; in the case of identical numbers of authors, the different citations should be listed by year.

Styles of citations in the reference list for books, articles, abstracts and proceedings are listed as follows:

a) books - surnames and initials of all the authors (in small capitals), year of publication (in brackets), full title (italicised), publisher and place of publication, pages; e.g., COX K.G., BELL J.D. and PANKHURST R.J. (1979) - *The interpretation of igneous rocks*. Chapman Hall, London, 450 p.

b) articles in journals - surnames and initials of all the authors (in small capitals), year of publication (in brackets), full title of the paper (italicised), name of the journal, volume (boldface), first and last page numbers; e.g., PASQUALI C. and TRAVERSA G. (1996) - *Petrography and mineral chemistry of late-Hercynian dykes from southern Corsica*. Per. Mineral., **65**, 213-256.

c) abstracts and proceedings of Conferences - surnames and initials of all the authors (in small capitals), year of publication (in brackets), full title of the abstract or proceedings (italicised), In: Official topic of the conference (in inverted commas and italicised), host journal, volume (boldface), first and last page numbers; e.g., STEVENSON R.J., DINGWELL D.B., BAGDASSAROV N.S. and WEBB S.L. (1995) - *Rheological modeling of an emplacing rhyolite lava flow: implication for hazard assessment*. In: "*Volcanoes in Town, an IAVCEI Conference on Volcanic Hazards in Densely Populated Regions*", extended abstract volume, Per. Mineral., **64**, 275-276.

7. Tables must be prepared for camera-ready printing.

Author(s) should take into consideration the limitations set by the size ($14 \, cm \times 18.5 \, cm$) of the "Periodico di Mineralogia". If many data are presented authors are invited to divide their data set into two or more tables. Tables should be ready for 1:1 reproduction. For editing their tables authors should use "Times New Roman" font with a size of 10 points. Footnotes of tables should be listed apart and provided along with original and copies of tables. Reference should be made in the text to each table. A list of captions would be furnished at the end of tables.

8. Illustrations (drawings and photographs) should respect the page format of the "Periodico di Mineralogia" ($14 \, cm \times 18.5 \, cm$). Lettering should also be as large as possible to allow for eventual reduction without becoming illegible. Colour illustrations can be accepted, and paid for by the author(s) (see below). Bar scales should be used rather than numeric scales, which must be changed in the case of reduction. All illustrations should be supplied in a camera-ready. References should be made in the text to each figure. Each illustration must be accompanied by a caption. A list of captions would be furnished at the end of illustrations.

Only one set of galley proofs will be sent to the author(s) to be checked only for typesetting/editing errors. The author(s) is (are) not expected to make changes or corrections that will modify the accepted version of the manuscript. Galley proofs should be returned within three days to: "TIPOGRAFIA BARDI" Piazza delle Cinque Lune, 113, I-00186 Rome, Italy.

Thirty reprints of each article are supplied free of charge. Additional copies may be purchased:

Pages	20 copies	50 copies	100 copies	150 copies	per 50 copies above 150
3 to 4	E 16,50	E 27,50	E 49,50	E 66,00	E 16,50
5 to 8	E 27,50	E 49,50	E 82,50	E 110,00	E 27,50
9 to 16	E 44,00	E 82,50	E 137,50	E 165,00	E 44,00
Per set of 8 above 16	E 16,50	E 27,50	E 49,50	E 66,00	E 17,50

Color prints are charged according to their dimensions: half column E 165,00; half page E 187,00; full page E 220,00.

Additional reprints can be ordered on a Reprint Order Form which will be sent to the corresponding author with proofs for correction.

Original drawings and photographs of papers published will be returned upon request by the author(s) within two months of publication date.

Manuscripts should be submitted either to the Scientific Editor (Lucio Morbidelli, Dipartimento di Scienze della Terra, Università degli Studi "La Sapienza", Piazzale Aldo Moro, 5, I-00185 Rome, Italy) or to one of the members of the Editorial Board (see inside cover).